Ca^{2+}–Calmodulin regulates SNARE assembly and spontaneous neurotransmitter release via v-ATPase subunit V0a1

Dong Wang,[1] Daniel Epstein,[1] Ossama Khalaf,[1] Sankaranarayanan Srinivasan,[3] W. Ryan Williamson,[1] Amir Fayyazuddin,[4] Florante A. Quiocho,[3] and P. Robin Hiesinger[1,2]

[1]Department of Physiology and [2]Green Center Division for Systems Biology, University of Texas Southwestern Medical Center, Dallas, TX 75390
[3]Verna and Marrs McLean Department of Biochemistry and Molecular Biology, Baylor College of Medicine, Houston, TX 77030
[4]Dart Neuroscience LLC, San Diego, CA 92131

Most chemical neurotransmission occurs through Ca^{2+}-dependent evoked or spontaneous vesicle exocytosis. In both cases, Ca^{2+} sensing is thought to occur shortly before exocytosis. In this paper, we provide evidence that the Ca^{2+} dependence of spontaneous vesicle release may partly result from an earlier requirement of Ca^{2+} for the assembly of soluble *N*-ethylmaleimide–sensitive fusion attachment protein receptor (SNARE) complexes. We show that the neuronal vacuolar-type H^+-adenosine triphosphatase V0 subunit a1 (V100) can regulate the formation of SNARE complexes in a Ca^{2+}–Calmodulin (CaM)-dependent manner. Ca^{2+}–CaM regulation of V100 is not required for vesicle acidification. Specific disruption of the Ca^{2+}-dependent regulation of V100 by CaM led to a >90% loss of spontaneous release but only had a mild effect on evoked release at *Drosophila melanogaster* embryo neuromuscular junctions. Our data suggest that Ca^{2+}–CaM regulation of V100 may control SNARE complex assembly for a subset of synaptic vesicles that sustain spontaneous release.

Introduction

Synaptic vesicle fusion is a tightly Ca^{2+}-regulated process at the heart of chemical communication between neurons (Schneggenburger and Neher, 2005; Rizo and Rosenmund, 2008; Südhof and Rothman, 2009; Jahn and Fasshauer, 2012). Different modes of synaptic vesicle fusion have been described, including evoked synchronous and asynchronous release (Sun et al., 2007; Yoshihara et al., 2010; Yao et al., 2011) and spontaneous single vesicle release (Xu et al., 2009; Groffen et al., 2010; Pang et al., 2011). The Ca^{2+}-sensing mechanism underlying synchronous release is well studied and based on the cooperation of SNARE-mediated membrane fusion with Synaptotagmin-1 and its homologues (Xu et al., 2007; Rizo and Rosenmund, 2008). Other Ca^{2+}-sensing proteins function in spontaneous and asynchronous release, but it is unclear whether these are sufficient to explain all Ca^{2+}-dependent release (Xu et al., 2009; Groffen et al., 2010; Johnson and Chapman, 2010; Pang et al., 2011; Yao et al., 2011).

CaM has been considered as a potential Ca^{2+} regulator in neurotransmitter release for many years (DeLorenzo, 1981; Steinhardt and Alderton, 1982). However, it is unclear whether the kinetics of Ca^{2+}–CaM regulation are consistent with fast regulation of vesicle fusion. In addition, CaM has a plethora of functions at synapses, making it difficult to pinpoint a single molecular target of CaM in neurotransmission (Di Giovanni et al., 2010b; Pang et al., 2010; Lipstein et al., 2013).

V0 subunits of the v-ATPase have repeatedly been suggested to play a role in membrane fusion independent of a role in acidification (Peters et al., 2001; Morel et al., 2003; Hiesinger et al., 2005; Liégeois et al., 2007; Peri and Nüsslein-Volhard, 2008; Di Giovanni et al., 2010a; Strasser et al., 2011). The neuronal V0 subunit a1 (V0a1; V100 in flies) interacts with SNARE

D. Wang and D. Epstein contributed equally to this paper.

Correspondence to P. Robin Hiesinger: robin.hiesinger@utsouthwestern.edu

O. Khalaf's present address is École Polytechnique Fédérale de Lausanne, 1015 Lausanne, Switzerland.

W.R. Williamson's present address is Janelia Farm Research Campus, Ashburn, VA 20147.

Abbreviations used in this paper: BLI, bilayer interferometry; CD, circular dichroism; EJC, excitatory junction current; ERG, electroretinogram; IP, immunoprecipitation; mEJC, miniature EJC; mEPC, miniature end plate current; NMJ, neuromuscular junction; n-Syb, neuronal Synaptobrevin.

The Rockefeller University Press $30.00
J. Cell Biol. Vol. 205 No. 1 21–31
www.jcb.org/cgi/doi/10.1083/jcb.201312109

proteins and plays a role on synaptic vesicles (Perin et al., 1991; Galli et al., 1996; Morel et al., 2003; Hiesinger et al., 2005) and endomembrane degradation in *Drosophila melanogaster* and zebrafish (Peri and Nüsslein-Volhard, 2008; Williamson et al., 2010). As in the case of CaM, the essential function of the v-ATPase is indispensable for a plethora of cellular processes (Nishi and Forgac, 2002). In particular, v-ATPase–dependent acidification can directly or indirectly affect secretion and membrane fusion, making it difficult to separate these functions in vivo (Saw et al., 2011; Ernstrom et al., 2012; Coonrod et al., 2013; Poëa-Guyon et al., 2013; Wang and Hiesinger, 2013). Recent evidence for separable function of V0a1/V100 in acidification and exocytosis comes from both genetic dissection using a selectively acidification-defective protein (Williamson et al., 2010) and temporal dissection using photoinactivation (Poëa-Guyon et al., 2013). However, the mechanism whereby V0a1/V100 may function in vesicle exocytosis independently of a role as part of the proton pump remains unclear.

In this study, we isolate and characterize a specific acidification-independent function of V100 that is regulated by Ca^{2+}–CaM. By doing so, we also isolate and characterize a highly specific Ca^{2+}-regulated CaM function at synapses that depends on a single target protein. We find that Ca^{2+}–CaM regulation of V100 is a positive regulator of SNARE complex assembly. Disruption of the Ca^{2+}–CaM regulation of V100 specifically abolishes >90% of spontaneous vesicle release at *Drosophila* embryo neuromuscular junctions (NMJs) but only has mild effects on evoked release. We propose a model whereby Ca^{2+}–CaM-dependent regulation of V100 may affect a subset of synaptic vesicles that underlie spontaneous release.

Results and discussion

V100 disrupts t-SNARE complex assembly, and Ca^{2+}-CaM binding releases this competition

We have previously shown that V100 directly binds to the t-SNAREs Syx1A (Syntaxin 1A) and SNAP25 individually (Hiesinger et al., 2005; Williamson et al., 2010) and to CaM in a Ca^{2+}-dependent manner (Zhang et al., 2008). Poor solubility of the N-terminal fragment of V100 that includes these binding sites has so far precluded more detailed biochemical interaction studies. To overcome this problem, we identified a partly hydrophobic 20–amino acid loop in the 407–amino acid *Drosophila* V100 N terminus that is not present in the orthologous proteins in yeast, worm, zebrafish, mouse, or human (Fig. S1 A). Deletion of this loop resulted in soluble, pure protein (Fig. S1 B) that was well folded as assessed by circular dichroism (CD) spectroscopy (Materials and methods; Fig. S1 C). Neuron-specific expression of *v100-Δloop* in the *v100*-null mutant rescues embryonic lethality to viable adults that are indistinguishable from wild type and exhibit normal neurotransmission (Fig. S1, D and E). We conclude that the properties required for normal V100 function are preserved in the V100N-Δloop protein (hereafter referred to as V100N).

A 133–amino acid V100 N-terminal fragment (amino acids 10–143) containing two coiled-coil domains (V100N-short) is sufficient for t-SNARE binding (Hiesinger et al., 2005). We now performed GST-Syx1A pull-downs of SNAP25 and the entire 407–amino acid V100N at varying ratios (Fig. 1 A). Surprisingly, increasing amounts of V100N reduced binding of SNAP25, and 1 µM V100N effectively prevented binding of 0.5 µM SNAP25. GST-SNAP25 pull-downs of Syx1A with increasing amounts of V100N showed the same competitive binding pattern (Fig. 1 B). Preincubation of SNAP25 with GST-Syx1A beads (preformed t-SNARE complexes) resulted in no significant alteration of the competitive binding behavior (Fig. 1 C). We conclude that V100N disrupts t-SNARE complexes in vitro. In contrast, V100N-short binds to both t-SNAREs even when added at eightfold concentrations without disrupting the t-SNARE complex (Fig. S2, A and B).

V100N contains a CaM binding domain (314N-333N) that is absent in V100N-short (Zhang et al., 2008). We hypothesized that CaM binding may affect V100N–t-SNARE interactions. Indeed, addition of Ca^{2+}–CaM fully relieved competitive binding of V100N and permitted simultaneous binding of V100N and SNAP25 to Syx1A, similar to V100N-short (Fig. 1 D). This effect was observed with 1 mM Ca^{2+} but increases to completion with 5 and 10 mM Ca^{2+} under our in vitro conditions (Fig. S2 C). We used the low 1 µM CaM concentration to match 1 µM V100N in all pull-downs in Fig. 1 and Fig. 2 and performed all subsequent experiments with 1 µM CaM and 5 mM Ca^{2+}. To test whether the Ca^{2+}–CaM effect is caused by binding to V100N, we made Ca^{2+}–CaM binding–deficient $V100N^{WFI}$ with three amino acids (W318, F319, and I328) replaced by alanine (Fig. S2 G). Ca^{2+}–CaM binding–deficient $V100N^{WFI}$ protein exhibited the same competitive binding properties as wild-type V100N in the absence of Ca^{2+}–CaM (Fig. 1 E), confirming that the Ca^{2+}–CaM interaction is not required for V100N–t-SNARE interaction per se. However, addition of Ca^{2+}–CaM in the presence of $V100N^{WFI}$ did not relieve the SNAP25 competition, indicating that the effect of Ca^{2+}–CaM on competitive binding is through direct interaction of CaM and V100N. The kinetics and specificity of this interaction were confirmed by bilayer interferometry (BLI; Fig. S2 D and Table S1) and pull-down experiments (Fig. S2, E–G). We conclude that Ca^{2+}-dependent binding of CaM to V100N releases competitive binding of V100N to Syx1A and SNAP25 and permits t-SNARE complex formation.

The competitive V100N binding to t-SNAREs was not altered even when an excess of the v-SNARE neuronal Synaptobrevin (n-Syb) was simultaneously added to the GST-Syx1A pull-down (Fig. 1 F). However, the competition was released when Ca^{2+}–CaM was added to the reaction (Fig. 1 F). In contrast, preformed v-/t-SNARE complexes were resistant to competitive binding of V100N (Fig. 1 G), consistent with the extraordinary stability of the ternary SNARE complex. These data suggest that V100N can disrupt SNARE complexes during assembly but not once they are formed.

To test which V100N–SNARE complexes occur in vivo, we performed coimmunoprecipitations (IPs; co-IPs) from homogenized fly brain tissue. We detected ∼1% of Syx1A and SNAP25 from total input but no detectable amount of n-Syb in complex with V100 (Fig. 2, A and B; and Fig. S2 H). This

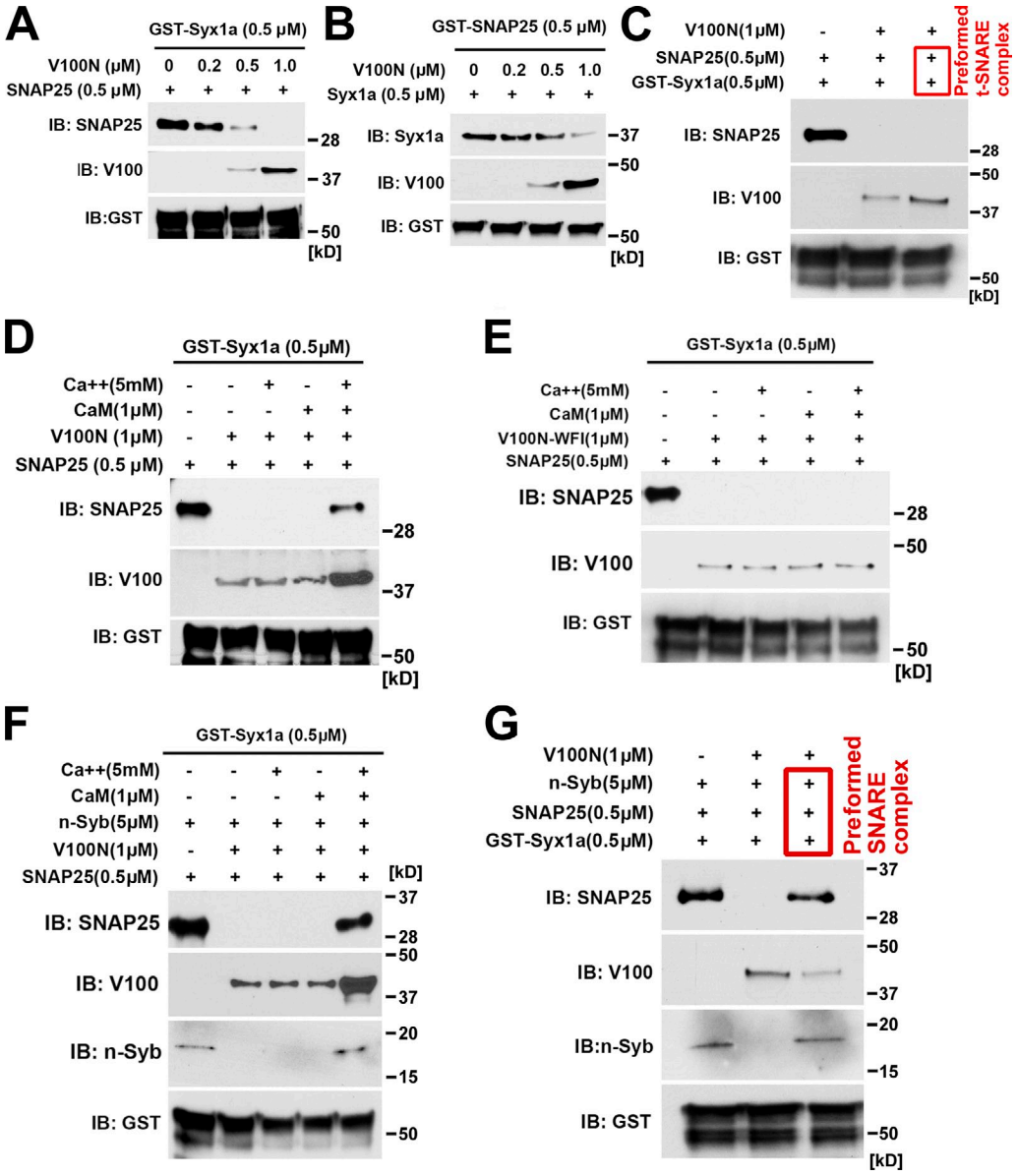

Figure 1. **The V100 N terminus competes with the t-SNARE interaction in a Ca^{2+}–CaM-dependent manner.** (A) GST-Syx1A pull-down reveals competitive binding of V100N and SNAP25 to Syx1A. V100N and His-SNAP25 were added simultaneously to GST-Syx1A beads at the indicated concentrations and incubated overnight at 4°C. Shown are immunoblots probed with anti-V100 and anti-SNAP25 antibodies. (B) GST-SNAP25 pull-down analogous to A. (C) V100N can disrupt preformed t-SNARE complexes. Preformed t-SNARE complexes were generated by incubating GST-Syx1A and His-SNAP25 overnight at 4°C. After washing twice in binding buffer, 1 μM V100N was added at 4°C for another 2 h. (D–F) Immunoblots after GST pull-downs with the indicated protein concentrations and experimentally analogous to A. (D) Ca^{2+}–CaM relieves competitive binding and increases both SNAP25 and V100N binding to Syx1A. (E) Loss of the Ca^{2+}–CaM binding site in the $V100N^{WFI}$ protein does not affect competitive binding but prevents Ca^{2+}–CaM-dependent release of competition. (F) Immunoblot after GST-Syx1A pull-down similar to D but including n-Syb. (G) Immunoblot after GST pull-down similar to C but with preformed SNARE complex including n-Syb. V100N does not efficiently disrupt a preformed full v-/t-SNARE complex. IB, immunoblot.

observation suggests that V100 in vivo is only bound to a small subset of t-SNAREs that are not bound to the v-SNARE n-Syb. Co-IPs probed for both proteins further indicated that ≤50% of the much less abundant V100 protein in fly brain is in a complex with Syx1A (Fig. S2 H).

The Syx1A H_{abc} domain is required for Ca^{2+}–CaM–V100N-dependent SNARE complex assembly

There are at least two possible explanations for the competitive binding of V100N: either V100N keeps Syx1A in a closed conformation, which prevents SNAP25 binding, or V100N directly competes with binding to the exposed SNARE domains. To distinguish between these possibilities, we first generated a constitutively "open" Syx1A protein that has previously been extensively characterized in *Caenorhabditis elegans* and mouse (Richmond et al., 2001; Gerber et al., 2008). As shown in Fig. 2 C, open Syx1A behaved identical to wild-type Syx1A in our V100N competition assay and exhibited a twofold increase of V100N binding after Ca^{2+}–CaM addition (Fig. 2, D and E). Because V100N binding is not altered by open Syx1A, we reasoned that V100N may directly

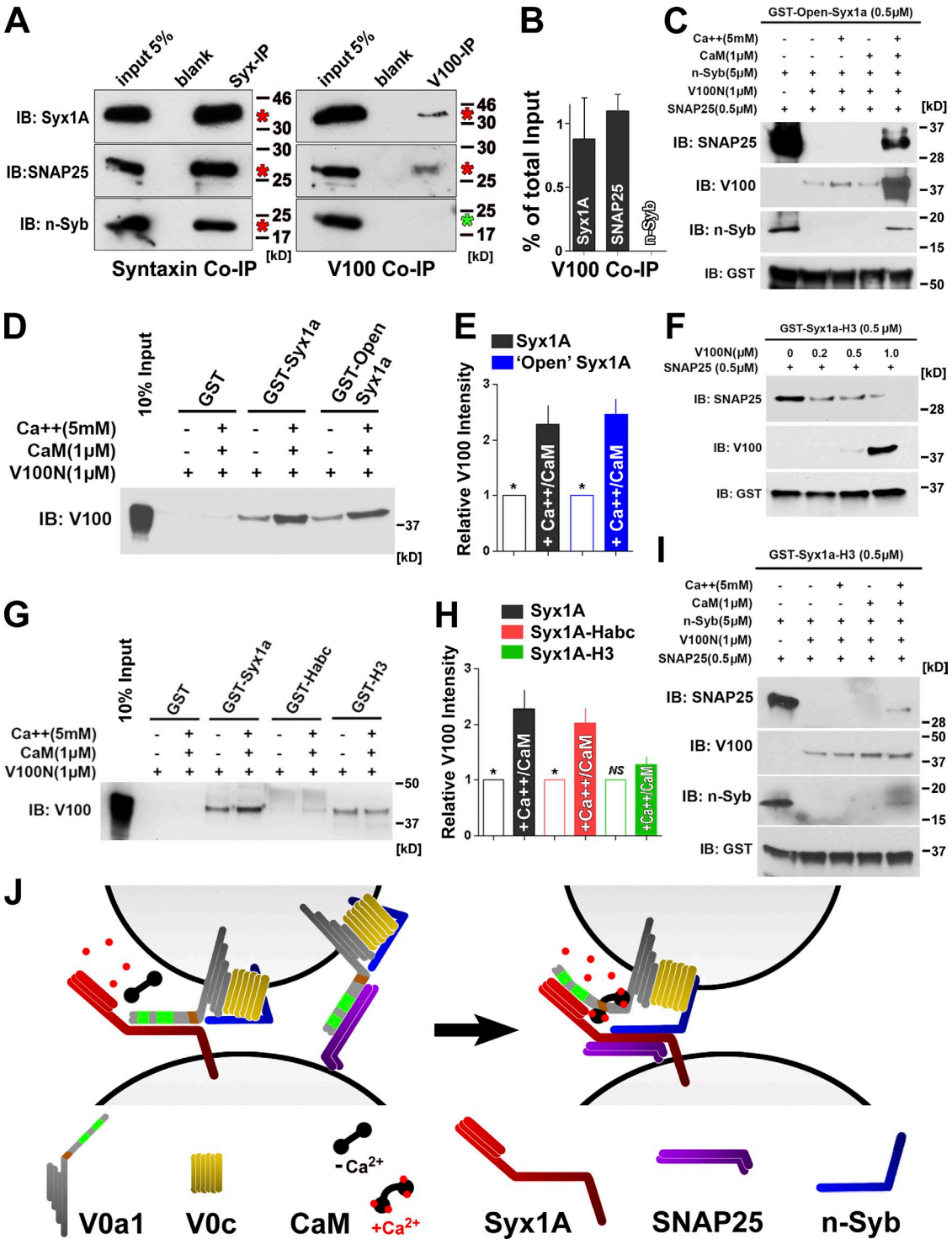

Figure 2. **V100N is a positive regulator of SNARE complex formation.** (A) Co-IP with the anti-Syx1A antibody from fly head extract shows amounts of interacting Syx1A, SNAP25, and n-Syb equivalent to the 5% input lane. In contrast, anti-V100 coimmunoprecipitates a smaller pool of t-SNAREs, and there is no detectable v-SNARE n-Syb. Red asterisks indicate the signals that can be detected by co-IP. The green asterisk indicates that there is no detectable n-Syb signal by V100 co-IP. (B) Quantification of three V100 co-IPs including the one shown in A. 0.5–1% of Syx1A and SNAP25, but no detectable n-Syb, is coimmunoprecipitated with V100. (C–I) Immunoblots after GST pull-downs of the indicated protein concentrations, added simultaneously and incubated overnight at 4°C. (C) The LE mutation in open Syx1A does not affect V100N competition and Ca^{2+}–CaM-dependent release. (D and E) Ca^{2+}–CaM increases binding of V100N to Syx1A and open Syx1A equally. Before versus after addition of Ca^{2+}–CaM, ~2% versus ~5% of total V100N input binds to GST-Syx1A. Input lane shows 10% of total input. (F) V100N binds competitively to Syx1A-H3 in the absence of the H_{abc} domain. (G and H) Ca^{2+}–CaM increases V100N binding to Syx1A and the H_{abc} domain in isolation but not to the H3 domain in isolation. (I) Ca^{2+}–CaM does not efficiently increase V100N binding and SNARE complex formation in the absence of the H_{abc} domain. (J) Working model for the transition from competitive V100N binding to Ca^{2+}–CaM-mediated full SNARE complex assembly. Note that our data do not distinguish between Syx1A and SNAP25 in the vesicle or target membrane. IB, immunoblot. Error bars show SEM. *, $P < 0.01$.

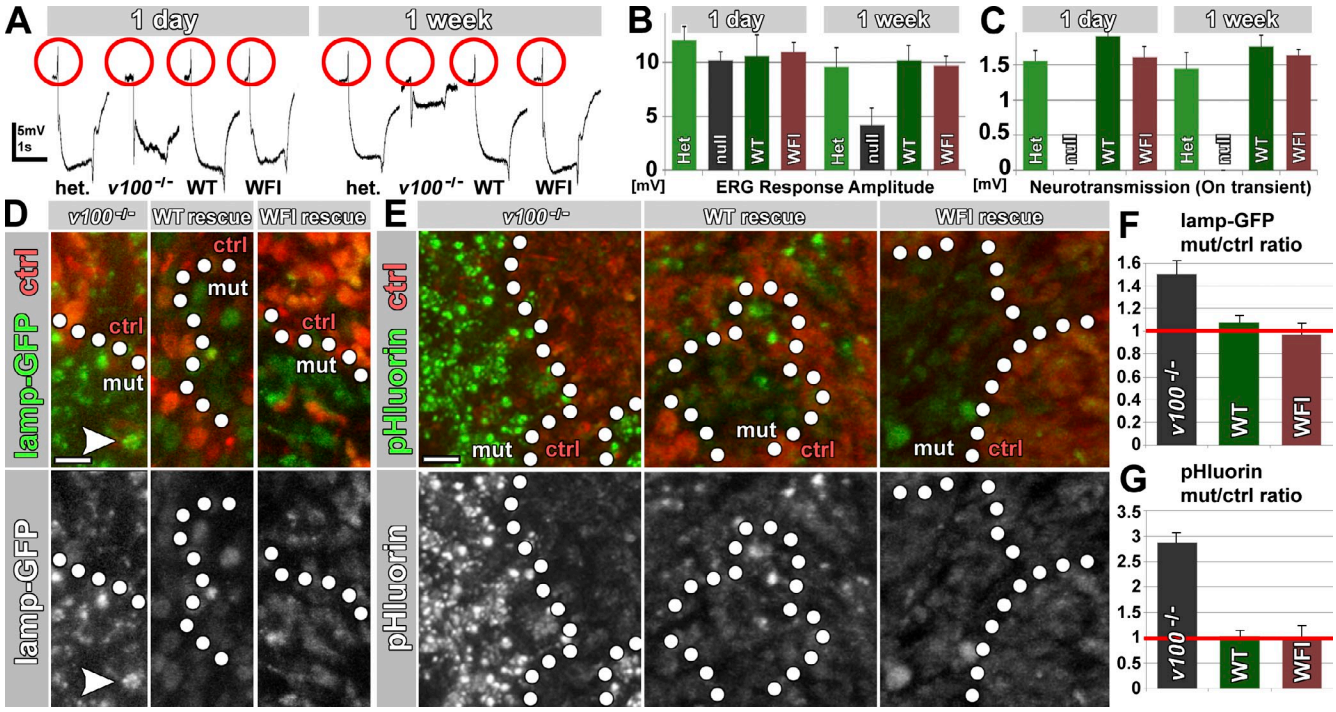

Figure 3. **CaM binding to V100 is not required for acidification, neurotransmission, or endolysosomal function in *Drosophila* photoreceptors.** (A) Representative electroretinogram (ERG) recordings of 1-d- and 1-wk-old flies with eyes of the indicated genotypes. Red circles indicate the transient on signal in ERG recordings. (B) Quantification of ERG response amplitudes. The null mutant shows a significantly reduced response amplitude after 1 wk as a result of photoreceptor degeneration, which is rescued with *v100*^{WFI}. (C) Quantification of ERG on transients reveals a neurotransmission defect that is fully rescued with *v100*^{WFI}. (D–G) Marked control (ctrl) and mutant (mut) photoreceptor synaptic terminals expressing lamp-GFP (D) or synaptopHluorin (E) with quantification in F and G, respectively. Lamp-GFP reveals endolysosomal accumulations and pHluorin endolysosomal acidification defects in the null mutant. Both are fully rescued with *v100*^{WFI}. Arrowheads in D indicate the accumulation of Lamp-GFP in the V100 mutant background but not seen in control cells. White dotted lines mark the outline of the boundaries between mutant and wild-type tissues. Bars, 2 µm. The red lines in F and G mark an equal ratio of the measured protein levels in mutant versus control cells. Error bars show SEM. Het, heterozygous; WT, wild type.

bind to the H3 (SNARE) domain or the N-terminal H_{abc} domain. Pull-downs using only the Syx1A SNARE domain (Syx1A-H3) revealed unaltered V100 binding competition, confirming that the competitive binding occurs directly at the SNARE domain and does not function through "closing" Syx1A (Fig. 2 F). However, addition of Ca^{2+}–CaM did not significantly increase binding of V100N to Syx1A-H3 (Fig. 2, G and H). These findings suggest that the H_{abc} domain is required in addition to the H3 domain in order for Ca^{2+}–CaM to function as a positive regulator of SNARE complex assembly (Fig. 2 I). In contrast to the H3 domain, V100N binding to the Syx1A H_{abc} domain in isolation exhibits almost no binding in the absence of Ca^{2+}–CaM. However, addition of Ca^{2+}–CaM permits weak binding to H_{abc}, even in the absence of other Syx1A domains (Fig. 2, G and H). These data support a model in which binding of Ca^{2+}–CaM to V100N alters the binding of V100N to Syx1A from exclusive H3 domain binding to a conformation that includes the H_{abc} domain (Fig. 2 J). In this model, Ca^{2+}–CaM binding to V100N functions as a positive regulator of SNARE complex formation after opening of Syx1A but before v-/t-SNARE–mediated membrane fusion (Fig. 2 J). We have previously shown that V100 only binds to specific syntaxins, including Syx1A and Syx7, but not, for example, Syx16 (Williamson et al., 2010). Ca^{2+}–CaM–V100 may thus regulate assembly of distinct subsets of SNARE complexes on distinct vesicles.

CaM binding to V100 is not required for acidification, endolysosomal function, or neuronal maintenance

We have previously shown that a CaM-binding mutant V100 variant did not rescue embryonic lethality, suggesting that Ca^{2+}–CaM regulation is critical for V100 function (Zhang et al., 2008). However, neither the mechanism nor the role of this regulation has been investigated because overexpression of Ca^{2+}–CaM binding–deficient V100 is toxic (Zhang et al., 2008). We therefore generated a new transgenic insertion of the CaM binding–deficient mutant *v100*^{WFI} through selection of a weak random *P* element insertion that allowed expression of $V100^{WFI}$ at endogenous levels (Fig. S3, A and B) and caused no obvious developmental defects (Fig. S3 C). The $V100^{WFI}$ protein localized to synapses in a manner indistinguishable from $V100^{WT}$ (Fig. S3, D and E). Furthermore, *v100*^{WFI} did not cause any obvious changes of the active zone marker Bruchpilot (nc82), the t-SNARE protein Syx1A, or the synaptic vesicle proteins n-Syb and Cysteine String Protein (Fig. S3, F and G).

Next, we tested which of the numerous V100 functions depend on Ca^{2+}–CaM regulation. Loss of *v100* causes photoreceptor neurotransmission defects (Hiesinger et al., 2005). Surprisingly, *v100*^{WFI} fully rescued this neurotransmission defect of *v100*-null mutant photoreceptors (Fig. 3, A and C). Loss of *v100* also causes endolysosomal defects that lead to slow,

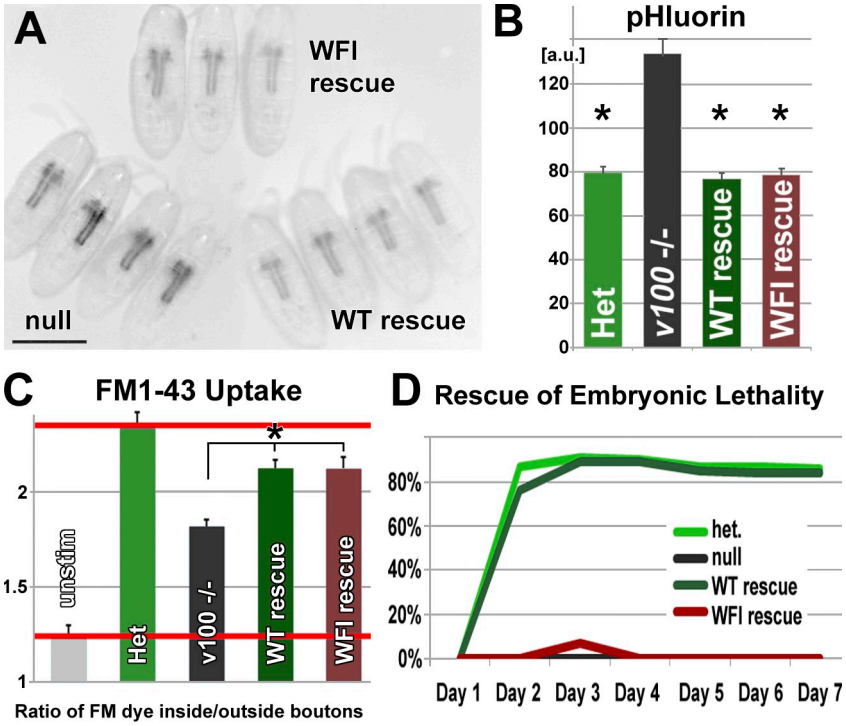

Figure 4. **CaM binding to V100 is required for viability but not for acidification or stimulated vesicle cycling in *Drosophila* embryos.** (A) Panneuronal synaptopHluorin expression in live embryos reveals increased fluorescence in null mutant embryos that is fully rescued with $v100^{WFI}$. (B) Quantification of synaptopHluorin acidification measurements. (C) Quantification of FM1-43 uptake experiments at the embryonic NMJ (≥10 embryos per genotype; representative images in Fig. S3 H). The bottom red line indicates the FM1-43 dye intensity before stimulation (background); the top red line indicates the maximum FM1-43 intensity observed in heterozygote control animals. (D) Survival curves of 100 embryos per genotype. Wild-type (WT) rescue and $v100^{WFI}$ (WFI) rescue reflect neuron-specific expression of each variant in a null mutant embryo. Asterisks denote significance in pairwise *t* tests with the null mutant. Bar, 200 µm. Error bars show SEM. a.u., arbitrary unit; Het, heterozygous; unstim, unstimulated.

adult-onset neurodegeneration (Williamson et al., 2010). Again, $v100^{WFI}$ fully rescued this defect (Fig. 3, A and B). Expression of $v100^{WFI}$ also fully rescued endolysosomal trafficking as visualized with lamp-GFP (Fig. 3, D and F). Finally, we directly tested a requirement of Ca^{2+}–CaM regulation of v-ATPase–dependent acidification through coexpression of the acidification-sensitive synaptopHluorin (Ng et al., 2002). Surprisingly, acidification defects of the null mutant are fully rescued by expression of $v100^{WFI}$ (Fig. 3, E and G). These results show that all previously reported defects of *v100*-null mutant photoreceptor neurons can be rescued by expressing Ca^{2+}–CaM binding–deficient $v100^{WFI}$ at endogenous levels.

To test v-ATPase–dependent acidification in the entire embryo, we expressed synaptopHluorin in all neurons. Similar to photoreceptor synapses, both $v100^{WT}$ and $v100^{WFI}$ equally rescued the acidification defect in the embryonic central nervous system (Fig. 4, A and B). These results corroborate that Ca^{2+}–CaM regulation of V100 is not measurably required for v-ATPase–dependent acidification. To assess defects in synaptic vesicle cycling, we assayed FM1-43 dye uptake at the embryonic NMJ. *v100*-null mutant embryos exhibited a ∼50% reduction in FM1-43 uptake, similar to previous measurements (Hiesinger et al., 2005). The FM1-43 uptake defect in the mutant is equally rescued by $v100^{WT}$ and $v100^{WFI}$ (Fig. 4 C and Fig. S3 H), suggesting that Ca^{2+}–CaM regulation is not required for *v100*-dependent synaptic vesicle cycling upon stimulation.

Expression of wild-type *v100* cDNA is sufficient to fully rescue the embryonic lethality of the *v100*-null mutant (Hiesinger et al., 2005). Based on the extensive rescue with $v100^{WFI}$ in both photoreceptors (Fig. 3) and in embryos (Fig. 4), we expected that panneuronal expression of $v100^{WFI}$ should also rescue embryonic viability. Surprisingly, our efforts to rescue embryonic lethality with $v100^{WFI}$ failed, in comparison to the robust rescue with $v100^{WT}$ (Fig. 4 D).

Ca^{2+}-CaM regulation of V100 is required for spontaneous neurotransmission

To identify the aspect of neuronal or synaptic function that is not rescued by $v100^{WFI}$, we performed electrophysiological recordings from NMJs in *Drosophila* embryos. As previously reported, presynaptic loss of *v100* resulted in a 50% evoked transmission failure rate and significantly reduced response amplitudes to <15% of wild type in the remaining excitatory junction currents (EJCs; Hiesinger et al., 2005; Fig. 5, A–C). However, we noticed that the very first evoked response often exhibited close to wild-type amplitudes (Fig. 5 C, arrow), which then rapidly dropped to <10% (without counting the 50% complete transmission failures). This phenotype was not previously observed and suggests that *v100* mutant synapses can elicit a strong EJC only once in response to a single action potential. Notably, $v100^{WFI}$ embryos also exhibited a drop of EJC amplitudes but, unlike the null mutant, plateaued around 40–50% of wild type after the third stimulus (Fig. 5, A–C). The 50% transmission failure rate of the null mutant was fully rescued by presynaptic expression of $v100^{WFI}$, similar to $v100^{WT}$ (Fig. 5, B and C). These findings suggest that Ca^{2+}–CaM regulation of V100 contributes to the availability of releasable vesicles but is not absolutely required for evoked neurotransmitter release.

Lastly, we analyzed spontaneous synaptic vesicle release events in the absence of stimulation. In the *v100*-null mutant, these miniature EJCs (mEJCs; <300 pA) are >90% reduced (Hiesinger et al., 2005). Remarkably, the mEJC frequency of

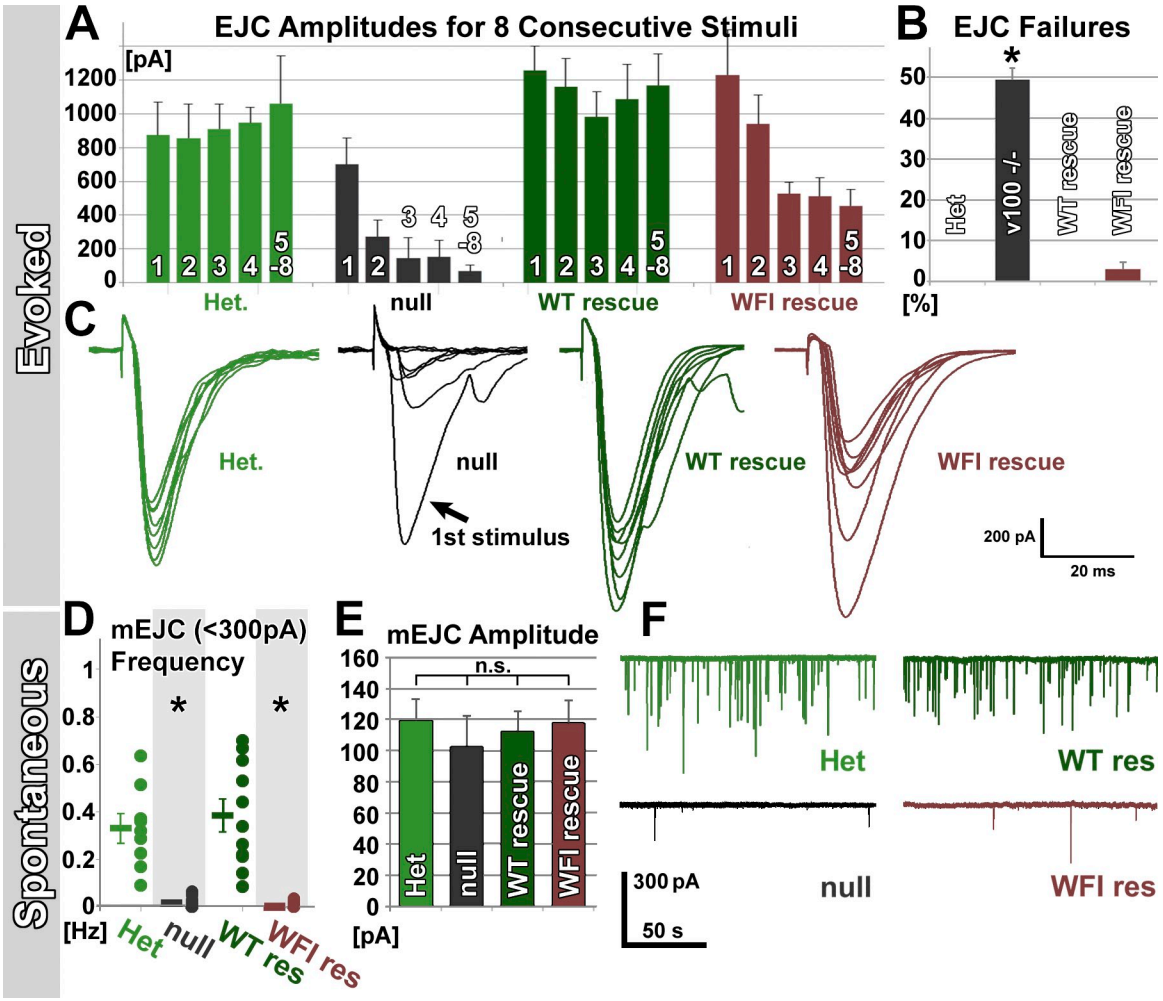

Figure 5. **Electrophysiological analysis at the embryonic NMJ reveals Ca^{2+}–CaM–V100 regulation of spontaneous vesicle release.** (A–C) Evoked synchronous release for the indicated genotypes. (A) Excitatory junctional currents (EJCs) after eight stimuli, one every 5 s. Complete transmission failure was not counted in A and is shown in B. Each column represents the mean amplitude of an evoked responses in a series of eight or more consecutive stimulations, where 1 is the mean of the responses to the first stimulation, 2 is the second, 3 is the third, 4 is the fourth, and 5–8 is the consolidation of the fifth–eighth consecutive stimulation. (B) A 50% transmission failure rate of the null mutant is rescued by presynaptic $v100^{WFI}$ expression. (C) Representative traces. (D–F) Spontaneous release for the indicated genotypes. (D) Frequency of mEJCs (<300 pA). (E) Amplitudes of mEJCs reveal no statistically significant differences, indicating normal neurotransmitter loading and vesicle acidification. (F) Representative mEJC traces. At least 10 embryos were recorded for each genotype and for evoked and spontaneous release separately. Asterisks denote significance in pairwise *t* tests with the heterozygous (Het) controls. Error bars show SEM. WT, wild type.

$v100^{WFI}$ is indistinguishable from the null mutant, whereas presynaptic $v100^{WT}$ expression fully rescued this phenotype (Fig. 5, D and F). The mEJC amplitudes are identical for the null mutant, $v100^{WFI}$, and $v100^{WT}$ rescues, consistent with our previous conclusion that acidification, and loading of synaptic vesicles with neurotransmitters does not require V100 (Fig. 5 E). We conclude that Ca^{2+}–CaM regulation of V100 has a mild effect on evoked transmission but is required for most spontaneous vesicle release. The precise role of mEJCs is still unclear, and their absence in the mutant, together with the reduced evoked responses and other potential neuronal defects not assayed here, may contribute to embryonic lethality.

To our knowledge, no other Ca^{2+}-regulating process or mutant has previously been shown to affect >90% of spontaneous release while only mildly affecting evoked release. The function of Ca^{2+}–CaM–V100 as a positive regulator of SNARE complex assembly may provide a potential mechanism for the specificity of this phenotype. Ca^{2+}-dependent regulation of V100 is highly unlikely to be required for all SNARE complex assembly because synchronous release is only mildly affected, and V100 is only associated with a subset of t-SNAREs that are not bound to v-SNAREs in vivo based on our co-IP experiments. A potential explanation for the differential effect on synchronous and spontaneous release modes could be the existence of different synaptic vesicle populations and vesicle-specific SNAREs (Sara et al., 2005; Ramirez and Kavalali, 2011). We have previously shown interaction specificity of V100 with different syntaxins (Williamson et al., 2010). Ca^{2+}–CaM–V100 regulation of SNARE complex assembly may only be required for a subset of vesicles that represent >90% of all the vesicles that are released spontaneously but can also be recruited to evoked synchronous responses upon repeated stimulation. This mechanism is consistent with the coexistence of Ca^{2+}-sensing mechanisms that acutely regulate vesicle fusion for all modes of

vesicle release. Alternatively, V100 may play a spatially restricted role at different release sites for spontaneous and evoked release (Melom et al., 2013). Ca^{2+}–CaM regulation of V100 may play little or no role in *Drosophila* photoreceptors because these are nonspiking neurons that release vesicles in response to graded potentials. It is unclear whether and how spontaneous release is regulated in these neurons.

Our model predicts that the Syx1A H_{abc} domain is required for Ca^{2+}–CaM–V100 regulation of SNARE assembly. If this mechanism underlies the neurotransmitter release phenotypes described here, a loss of the H_{abc} domain should specifically affect spontaneous neurotransmission. Indeed, a recent study in cultured cortical neurons showed that H_{abc} deletion causes a decrease in spontaneous release, indicating the essential role of Syx1A H_{abc} domain in spontaneous neurotransmission (Zhou et al., 2013).

Our findings bear similarity to the recently reported Ca^{2+}–CaM regulation of the synaptic vesicle binding protein Munc13-1, which, like *v100* and *v100^{WFI}*, exhibited a stimulation-dependent reduction of releasable vesicles (Lipstein et al., 2013). Recovery experiments like the ones presented in this study cannot easily be performed over the same time periods at the embryonic NMJ. However, over the 5-min period of acceptable patch clamp recording at the *Drosophila* embryonic NMJ, we never observed vesicle replenishment or recovery of the EJC amplitude in the *v100* and *v100^{WFI}* mutants. Lastly, the Ca^{2+}–CaM regulation described here does not argue for or against a potential role of V100 or other V0 subunits in the actual fusion reaction but specifically reveals an additional Ca^{2+}-regulatory mechanism upstream of exocytosis.

Materials and methods

Immunohistochemistry, microscopy, live imaging, and image processing

Embryo filets, adult brains, and pupal eye–brain complexes were dissected as previously reported (Hiesinger et al., 2005; Williamson and Hiesinger, 2010). For fixed imaging, the tissues were fixed in PBS with 3.5% formaldehyde for 15 min and washed in PBS with 0.4% Triton X-100. Specimens were mounted in Vectashield H-1000 mounting medium. High-resolution light microscopy was performed using a resonance scanning confocal microscope (SP5; Leica) with a 63×, NA 1.3 glycerine immersion lens (20×, NA 0.9 for low-resolution scans). Imaging data were processed and quantified using Amira 5.2 (Indeed) and Photoshop CS6 (Adobe). All confocal data are shown as single confocal sections or simple maximum intensity projections. Fluorescence data and electroretinogram (ERG) data were quantified using Prism 4 (GraphPad Software). Antibodies against Cysteine String Protein (ab49 mouse monoclonal), nc82 (mouse monoclonal), and Syx1A (8C3, mouse monoclonal; all obtained from the Developmental Studies Hybridoma Bank at the University of Iowa) were used at 1:50, anti–n-Syb (R29, rat; gift from H. Bellen, Baylor College of Medicine, Houston, TX; Wu et al., 1999) was used at 1:250, and anti-V100 (gp11 guinea pig polyclonal; Hiesinger et al., 2005) was used at 1:2,000. Secondary antibodies were tagged with Alexa Fluor 488, Cy3, or Cy5 fluorochromes.

For synaptopHluorin live imaging, developing eye–brain complexes were prepared in HL3 and immobilized on a coverslip coated with Sylgard as previously published (Williamson and Hiesinger, 2010; Williamson et al., 2010). The coverslip was then placed in a perfusion chamber (RC-30; Harvard Apparatus) with slow perfusion of HL3 solution. Images were captured using resonance scanning confocal microscopy (SP5). The same x/y region was captured for each scan from individual experiments. The data were processed in Amira 5.2.

ERGs

ERGs were performed as described in Fabian-Fine et al. (2003) with the following modifications: Flies were fixed using nontoxic Glue-All (Elmer's). We used 2 M NaCl in the recording and reference electrodes. Electrode voltage was amplified by a digital board (Digidata 1440A; Molecular Devices), filtered through an intracellular electrometer (IE-210; Warner Instruments), and recorded using Clampex 10.1 (Axon Instruments). A postrecording filter was also provided by the Clampex software. Light stimulus was provided in 1-s pulses by a computer-controlled white light-emitting diode system (MC1500; Schott).

FM1-43 uptake

FM1-43 uptake experiments were performed according to our previously published protocol (Hiesinger et al., 2005). In brief, embryo fillets were exposed to 10 µM FM1-43FX with or without 30 mM K^+ for 5 min and washed with ice-cold zero Ca^{2+} saline for 5 min containing 0.5 mM EGTA and 1 mM Advasep-7 (Biotium). Embryo fillets were fixed and stained for 5 min with concentrated HRP antibody (1:10) in the absence of detergent and subsequently with highly concentrated Cy5-conjugated secondary antibody. 3D confocal high-resolution datasets were obtained immediately after staining because, in our hands, the fixed FM1-43FX loses >50% fluorescence within 24 h. The surface of HRP-demarcated boutons was reconstructed and the mean voxel intensity in the FM1-43 channel calculated for the total volumes inside (boutons) and outside (muscle). Finally, inside/outside ratios were calculated and are presented in Fig. 4 C. At least 10 embryos were analyzed per genotype.

***Drosophila* embryo patch clamp**

Embryos were selected and dissected as described in Featherstone et al. (2009). All experiments were performed using embryos between 18 and 24 h after egg laying. Embryos were dissected in ice-cold HL3 solution containing (mM): 70 NaCl, 5 KCl, 11 $MgCl_2$, 10 $NaHCO_3$, 5 trehalose, 115 sucrose, 5 Hepes, and 0.5 $CaCl_2$, pH 7.2 (Stewart et al., 1994; Broadie et al., 1995; Hiesinger et al., 2005). A water-polymerizing cyanoacrylate glue was used to affix the embryo to Sylgard-coated coverslips. After the dissection, embryos were rinsed in PBS to remove HL3. The embryos were then treated with 1 mg/ml Collagenase type 1A (Sigma-Aldrich) in ice-cold HL3 lacking Ca^{2+} and Mg^{2+} for a duration of 0.5–2 min. Lastly, embryos were then rinsed three times with HL3 to inactivate the collagenase.

Whole-cell patch clamp recordings were made from muscle 6 of segments 2–4 using an amplifier (Multiclamp 700B; Molecular Devices) and a digital board (Digidata 1440A). Thin-walled (inner diameter of 1.2 mm; Sutter Instrument) borosilicate pipettes were pulled and fire polished to a 1–2-µm inner diameter with a resistance between 3 and 5 MΩ. Recording electrodes were filled with the following solution (mM): 120 KCl, 20 KOH, 4 $MgCl_2$, 0.25 $CaCl_2$, 5 EGTA, 24 sucrose, 5 Hepes, and 4 Na_2ATP. The muscles were voltage clamped at −60 mV.

Miniature end plate currents (mEPCs) and spontaneous end plate currents were recorded in HL3 at room temperature for 300 s using Clampex 10.3. HL3 was used for the relative dampening of spontaneous evoked activity, essentially as in Hiesinger et al. (2005) except that tetrodotoxin was not added to the solution. Only events between 30 and 300 pA were counted as mEPCs; the mean frequency and amplitude of these events were similar to previous measurements (Broadie et al., 1995; Featherstone et al., 2001; Chen et al., 2009). The mEPC amplitudes were measured using the template search option in Clampfit 10.3.

Evoked synaptic events were recorded at 18°C in standard saline, which was modified from Broadie et al. (1995) and contained (mM): 135 NaCl, 5 KCl, 4 $MgCl_2$, 1.8 $CaCl_2$, 72 sucrose, and 5 TES, pH 7.2. This saline was used for evoked recordings to eliminate the dampening effect of HL3 on evoked activity. The NMJ was stimulated through a suction electrode filled with bath solution, placed on the motor nerve as it exited the ventral nerve cord. Stimuli of 100-µs duration with an amplitude of 3–5 V were provided through a stimulus isolator every 5 s (0.2 Hz) as described in Hiesinger et al. (2005). Amplitudes of evoked responses were measured using the cursor tool of Clampfit 10.3.

Co-IPs

Total proteins were extracted from adult fly heads in IP buffer containing 20 mM Tris, 150 mM NaCl, 1 mM PMSF, and complete protease inhibitors (Roche), pH 7.4. The fly head extract was mixed well in 1% Triton X-100 (Bio-Rad Laboratories) and incubated for 1 h at 4°C. Samples were centrifuged at 16,000 *g* for 15 min at 4°C to remove cell debris. The resulting supernatant was incubated with 20 µl anti-V100 antibody and 8C3 anti-Syx1A antibody (Hiesinger et al., 2005) coupled to protein A/G beads (Santa Cruz Biotechnology, Inc.) for 1 h at 4°C. After removing the supernatant, the beads were washed four times with the IP buffer.

A noncoupled protein A/G bead was used as a control. The immunoprecipitates were eluted by boiling the beads in 50 µl SDS sample buffer and were then analyzed by Western blotting with 8C3 anti-Syx1A (1:2,000; mouse monoclonal antibody obtained from the Developmental Studies Hybridoma Bank at the University of Iowa), anti-SNAP25 (1:5,000; rat polyclonal obtained from H. Bellen; Wu et al., 1999), anti–n-Syb (1:5,000), and anti-V100 (1:5,000; guinea pig polyclonal gp11) antibodies (Hiesinger et al., 2005).

Generation and purification of V100 N-terminal protein (V100N) and CD spectroscopy

Attempts to obtain the 407–amino acid V100 fragment comprising the entire cytoplasmic N terminus led to insoluble protein. We identified a 20–amino acid loop in the *Drosophila* V100 N terminus that is not present in the orthologous proteins in yeast, worm, zebrafish, mouse, or human (Fig. S1 A). Deletion of this loop (spanning from 142S to 163Q) resulted in soluble, pure protein composed of residues 10–407. CD spectra showed characteristic double minima at 208 and 222 nm, indicating significant α-helical character (Fig. S1 C). The calculated helical content of 49% is close to the predicted value of 57%, further suggesting that the purified V100N-Δloop was properly folded.

Far-UV CD spectra (190–260 nm) of V100N at a concentration of 0.5 mg/ml in 20 mM sodium phosphate and 100 mM NaCl, pH 7.5, were collected on a CD spectrometer (J-815; JASCO) using a 0.1-cm quartz cuvette at 25°C. Spectra were collected 10 times in a continuous scanning mode at a speed of 200 nm/min with a bandwidth of 2 nm and data pitch of 0.5 nm. A baseline correction of buffer without protein was applied to subtract for background. Data were processed using the instrument software with means movement, curve smoothing, and a convolution width of 5. Dicroprot was used to calculate the secondary structure content (Deléage and Geourjon, 1993).

Generation of V100 mutant rescue constructs and transgenic lines

To generate a full-length *v100-Δloop* transgenic rescue construct, two pairs of PCR primer sets (primer 1 [P1], 5′-GGGGGAATTCATGGGTTCCCTATTCCGCAGCG-3′, and reverse primer 1 [R1], 5′-GTCCTCGTTTTGGTTGTCGGCCATCTCATCGAAGAACACTTGGG-3′, corresponding to V100 M1-E141 and P2, 5′-CCCAAGTGTTCTTCGATGAGATGGCCGACAACCAAAACGAGGAC-3′, and R2, 5′-GGGGCTCGAGTTACTCCTCGGCGGCGGCAGC-3′, corresponding to V100 M164-E856) were used to generate two DNA fragments. The resulting DNA fragments were used for SOEing (splicing by overlap extension) PCR to generate full-length *v100-Δloop* cDNA with primer sets P1 and R2. Full-length *v100* cDNA in a pOT2 vector (Berkeley Drosophila Genome Project clone LD21248) was used as a PCR template. The Ca^{2+}–CaM interaction mutant $v100^{WF}$ mutant (W318 and F319) was described previously (Zhang et al., 2008). The $v100^{WFI}$ mutant (W318, F319, and I328) was created to abolish any potential CaM binding to the predicted binding motif (Fig. S1 A). We used site-directed mutagenesis using full-length V100 cDNA and the following primers: 5′-GAATCTTAAGAACgcGgcCGTCAAGGTGCGCAAGATAAAGGCCgcCTACCATACGCTG-3′ (lowercase letters indicate the mutated nucleotides in the final mutant sequences) and its reverse complement. Transgenic expression of $v100^{WF}$ and $v100^{WFI}$ in *Drosophila* behaved identical in all assays, including transgenic rescue and overexpression experiments, electrophysiology, and immunohistochemistry. All mutant constructs were introduced into the pUAST vector by conventional PCR and ligation procedure and sequenced to confirm the presence of designed mutations. Transgenic lines bearing these constructs were generated by Rainbow Transgenic Flies, Inc. and maintained at room temperature unless indicated otherwise.

Generation of bacterial expression constructs and protein purification

All sequences are obtained from *Drosophila*. To make the His-tagged V100N-short fragments, we used the N-terminal 180 amino acids, which contain two predicted coiled-coil domains and had been shown previously to bind to Syx1A in vitro (Hiesinger et al., 2005). The following primers were used for this purpose: forward primer, 5′-GGGGGGATCCATGGGTTCCCTATTCCGCAG-3′, and reverse primer, 5′-GGGGCTCGAGCTCCTCGCCCAGCAGCTGCG-3′. The resulting PCR products were cloned into pET28a (EMD Millipore) to make His-tagged fusion proteins. The DNA sequence of V100 (fly subunit a1) corresponding to residues 10–407 with a loop deletion of residues spanning from 142S to 163Q (V100N) was amplified by PCR and cloned into the pET44 plasmid. $V100N^{WFI}$ was created in the same way as V100N and cloned into the pET44 plasmid, except the three amino acids (W318, F319, and I328) in the CaM binding domain were replaced with alanine (Zhang et al., 2008). Furthermore, we also created another single amino acid mutation, $V100N^{F}$, in which only F319 was replaced with alanine. $V100N^{F}$ has previously been shown to disrupt CaM binding to V100 as well and behaved identically in the biochemical assays (Zhang et al., 2008). Full-length fly CaM (residues 1–149) was cloned into the pET28a vector using the following primers: forward, 5′-GGGGGGATCCATGGCCGATCAGCTGACAGA-3′, and reverse, 5′-GGGGCTCGAGCTTCGATGTCATCATAGTCA-3′.

For the generation of Syx1A-GST fusion constructs, the following primers were used: Syx1A (1–267 aa) forward, 5′-GGGGGGATCCATGACTAAAGACAGATTAGC-3′, and reverse, 5′-GGGGCTCGAGCTTTCGTCGGGCTTTACTC-3′; Syx1A-H_{abc} (1–200 aa) forward, 5′-GGGGGGATCCATGACTAAAGACAGATTAGC-3′, and reverse, 5′-GGGGCTCGAGGGCCTCAATGTCCGCCAGCG-3′; and Syx1A-H3 (200–267 aa) forward, 5′-GGGGGGATCCCGCCACCAGGACATCATGAAG-3′, and reverse, 5′-GGGGCTCGAGCTTTCGTCGGGCTTTACTC-3′. For the open Syx1A/Syx1A L168A/E169A mutant (1–267 aa), the following primers were used to introduce the mutations: 5′-AACGACGATGAGGCGGCGAAGATGCTGGAG-3′ and its reverse complement. SOEing PCR was performed to make the Syx1A open mutant. For the SNAP25-GST fusion construct, the following primers were used: forward, 5′-GGGGGAATTCCCAGCGGATCCATCTGAAGAAGTTG-3′, and reverse, 5′-GGGGCTCGAGTTACTTTAATAGTTGATGTGCCC-3′. All GST fusion constructs were cloned into pGEX 4T-1 vector (GE Healthcare) and sequenced. The constructs of His-SNAP25 and His–n-Syb were generated as follows and described previously (Wu et al., 1999; Hiesinger et al., 2005): The *SNAP25* open reading frame was subcloned using EcoRI–XhoI into pET28c (EMD Millipore). *n-syb* (amino acids 1–104) was subcloned using BamHI–NdeI into pET28a (EMD Millipore). The plasmids were introduced into bacterial strain BL21 for expression and purification of target proteins.

Protein expression and purification were performed according to the following standard procedures: Overnight bacterial culture was transferred into fresh lysogeny broth medium at a 1:100 ratio and incubated at 37°C until OD_{600} reached 0.6. Next, the culture was induced with IPTG (0.5–1 mM for pET28a and pET44; 0.1 mM for pGEX 4T-1) at 19°C overnight. The overnight culture was collected by spinning in a rotor (JLA-8.1000; Beckman Coulter) at 5,000 rpm at 4°C for 15 min. The pellet was resuspended in 10 ml standard buffer (20 mM Tris/100 mM NaCl, pH 7.4) and lysed with BugBuster, 2 µl benzonase (EMD Millipore), and protease inhibitor cocktail (Roche) 10–20 min at room temperature. The lysate was centrifuged for 20 min at 16,000 rpm to remove cell debris. The supernatant was kept for protein purification.

For His-tagged proteins, cell lysate was bound to preequilibrated TALON resin followed by extensive washing with 10 mM imidazole, 300 mM NaCl, and 20 mM Tris, pH 7.5. This was followed by elution with 200 mM imidazole, 300 mM NaCl, and 20 mM Tris, pH 7.5. His-CaM was very pure after TALON resin and did not require further purification. Ion-exchange chromatography was performed on His-Syx1A and His-SNAP25 using a prepacked 5-ml HiTrap Q HP column (GE Healthcare) and eluted using a linear gradient of NaCl from 0.05 to 1 M, and pure fractions were pooled and concentrated. For GST-tagged proteins, cell lysate was incubated with glutathione beads followed by sequentially washing with PBS + 140 mM NaCl, pH 7.2, and PBS + 1 M NaCl, pH 7.2. GST-tagged proteins were eluted with 50 mM glutathione and 20 mM Tris, pH 8.0.

For Nus tag V100N (in pET44 plasmid) proteins, cell lysate was loaded onto preequilibrated TALON resin (Takara Bio Inc.). Resin was washed with 10 column volumes of 10 mM imidazole, 300 mM NaCl, and 20 mM Tris, pH 7.5. 1:50 ratio of thrombin (Haematologic Technologies, Inc.)/fusion protein was added to the resin and incubated with gentle shaking at room temperature for 2 h. The protein was eluted in 300 mM NaCl and 20 mM Tris, pH 7.5, and then, buffer was exchanged to 50 mM NaCl and 20 mM Tris-HCl, pH 8.0. Protein was bound to a prepacked 5-ml HiTrap Q HP column and eluted using a linear gradient of NaCl from 0.05 to 1 M. Fractions containing protein were pooled, concentrated by ultrafiltration, and further purified using a Superdex 200 HR16/60 column (GE Healthcare) in 50 mM NaCl and 20 mM Tris-HCl, pH 8.0. Pooled fractions were concentrated by ultrafiltration.

GST pull-down assays

For GST pull-down assays, the indicated GST fusion proteins were first bound to glutathione–Sepharose 4B (GE Healthcare) and subsequently washed with standard buffer (20 mM Tris/100 mM NaCl, pH 7.4) twice. The binding assay was performed with the indicated proteins added simultaneously together in binding buffer (20 mM Tris/150 mM NaCl,

pH 7.4/0.2% Triton X-100) incubated at 4°C overnight, with the following exceptions: To prepare preformed t-SNARE and preformed full SNARE complexes, we first added either His-tagged SNAP25 alone or together with n-Syb into the binding buffer containing GST-Syx1A beads. After an overnight incubation at 4°C, beads were spun down and briefly washed twice with binding buffer. Next, V100N was added into the preformed t-SNARE/full SNARE complex solution to perform the competition test for another 2 h at 4°C. After binding, the beads were washed three times in binding buffer. Proteins were eluted from GST beads with 100 mM glutathione/50 mM Tris/150 mM NaCl, pH 8.0. Eluted proteins were mixed with 4× SDS sample buffer for SDS-PAGE and Western blotting.

Octet (BLI) experiments

All BLI measurements were made on a biosensor instrument (Octet QK; ForteBio) using Ni–nitrilotriacetic acid sensors (Abdiche et al., 2008). Assays were performed in 96-well microplates at 25°C. All volumes were 200 µl. Baseline, loading, association, and dissociation steps for His-tagged Syx1A and SNAP25 onto nitrilotriacetic acid sensors was performed in 100 mM NaCl and 10 mM Hepes, pH 7.5. For His-CaM measurements, the same buffer with 5 mM $CaCl_2$ was used for the first three steps, and dissociation was carried in buffer without $CaCl_2$. 20 µg/ml His-tagged proteins were loaded onto the sensor for affinity measurements. Loading of His-tagged proteins was confirmed by changes in wavelength in the sensogram. Varying analyte concentrations of V100N were used for calculating the corresponding K_d values. Samples were clear, and no aggregation was observed. Sensors were recharged by a series of dips in 10 mM glycine, pH 1.7, and buffer, with a final dip in 10 mM $NiCl_2$. All measurements were performed three times with sequential recharging of sensors. Each measurement was subtracted for a baseline in which no V100N was added. Octet data analysis software was used to calculate the steady-state change in wavelength (response) for the corresponding association and dissociation times. K_d values and k_{on} rates were calculated using Octet data analysis software by fitting to a single site 1:1 binding function with the R^2 values indicated in Table S1. Other fitting stoichiometries did not provide good fitting for the data obtained. Experiments to obtain K_d values for Syx1A–SNAP25 interactions did not yield a curve that could be saturated, and Table S1 shows a comparison with previously published values using pull-down assays (Rickman et al., 2004).

Online supplemental material

Fig. S1 shows that deletion of a partially hydrophic 20–amino acid loop allows purification of a soluble 407–amino acid N-terminal protein and does not affect the in vivo function of full-length V100. Fig. S2 shows supplementary biochemical interaction experiments. Fig. S3 shows that the generation of CaM binding–deficient $V100^{WFI}$ with low expression at endogenous levels localizes to synapses, does not disrupt synaptic protein localization, and rescues FM1-43 uptake. Table S1 shows binding of V100N to Syx1A, SNAP25, and Ca^{2+}–CaM based on BLI. Online supplemental material is available at http://www.jcb.org/cgi/content/full/jcb.201312109/DC1.

We are grateful to Dr. David Featherstone for help with the electrophysiology. We thank Hugo Bellen, the Bloomington Stock Center, and the University of Iowa Developmental Studies Hybridoma Bank for reagents. We further thank Jose Rizo-Rey, Christian Rosenmund, Tanja Rosenmund, Reinhard Jahn, Ege Kavalali, and Christopher Peters for critical reading of this manuscript and all members of the Quiocho and Hiesinger laboratories for discussion.

This work was supported by grants from the National Institutes of Health to P.R. Hiesinger (RO1EY018884) and to F.A. Quiocho (5R01-GM088803) and the Welch Foundation to P.R. Hiesinger (I-1657) and F.A. Quiocho (Q-581).

The authors declare no competing financial interests.

Submitted: 23 December 2013
Accepted: 6 March 2014

References

Abdiche, Y., D. Malashock, A. Pinkerton, and J. Pons. 2008. Determining kinetics and affinities of protein interactions using a parallel real-time label-free biosensor, the Octet. *Anal. Biochem.* 377:209–217. http://dx.doi.org/10.1016/j.ab.2008.03.035

Broadie, K., A. Prokop, H.J. Bellen, C.J. O'Kane, K.L. Schulze, and S.T. Sweeney. 1995. Syntaxin and synaptobrevin function downstream of vesicle docking in *Drosophila*. *Neuron*. 15:663–673. http://dx.doi.org/10.1016/0896-6273(95)90154-X

Chen, K., D.E. Featherstone, and K. Broadie. 2009. Electrophysiological recording in the *Drosophila* embryo. *J. Vis. Exp.* e1348.

Coonrod, E.M., L.A. Graham, L.N. Carpp, T.M. Carr, L. Stirrat, K. Bowers, N.J. Bryant, and T.H. Stevens. 2013. Homotypic vacuole fusion in yeast requires organelle acidification and not the V-ATPase membrane domain. *Dev. Cell*. 27:462–468. http://dx.doi.org/10.1016/j.devcel.2013.10.014

Deléage, G., and C. Geourjon. 1993. An interactive graphic program for calculating the secondary structure content of proteins from circular dichroism spectrum. *Comput. Appl. Biosci.* 9:197–199.

DeLorenzo, R.J. 1981. The calmodulin hypothesis of neurotransmission. *Cell Calcium*. 2:365–385. http://dx.doi.org/10.1016/0143-4160(81)90026-9

Di Giovanni, J., S. Boudkkazi, S. Mochida, A. Bialowas, N. Samari, C. Lévêque, F. Youssouf, A. Brechet, C. Iborra, Y. Maulet, et al. 2010a. V-ATPase membrane sector associates with synaptobrevin to modulate neurotransmitter release. *Neuron*. 67:268–279. http://dx.doi.org/10.1016/j.neuron.2010.06.024

Di Giovanni, J., C. Iborra, Y. Maulet, C. Lévêque, O. El Far, and M. Seagar. 2010b. Calcium-dependent regulation of SNARE-mediated membrane fusion by calmodulin. *J. Biol. Chem.* 285:23665–23675. http://dx.doi.org/10.1074/jbc.M109.096073

Ernstrom, G.G., R. Weimer, D.R. Pawar, S. Watanabe, R.J. Hobson, D. Greenstein, and E.M. Jorgensen. 2012. V-ATPase V1 sector is required for corpse clearance and neurotransmission in *Caenorhabditis elegans*. *Genetics*. 191:461–475. http://dx.doi.org/10.1534/genetics.112.139667

Fabian-Fine, R., P. Verstreken, P.R. Hiesinger, J.A. Horne, R. Kostyleva, Y. Zhou, H.J. Bellen, and I.A. Meinertzhagen. 2003. Endophilin promotes a late step in endocytosis at glial invaginations in *Drosophila* photoreceptor terminals. *J. Neurosci.* 23:10732–10744.

Featherstone, D.E., W.S. Davis, R.R. Dubreuil, and K. Broadie. 2001. *Drosophila* alpha- and beta-spectrin mutations disrupt presynaptic neurotransmitter release. *J. Neurosci.* 21:4215–4224.

Featherstone, D.E., K. Chen, and K. Broadie. 2009. Harvesting and preparing *Drosophila* embryos for electrophysiological recording and other procedures. *J. Vis. Exp.* 27:e1347.

Galli, T., P.S. McPherson, and P. De Camilli. 1996. The V0 sector of the V-ATPase, synaptobrevin, and synaptophysin are associated on synaptic vesicles in a Triton X-100-resistant, freeze-thawing sensitive, complex. *J. Biol. Chem.* 271:2193–2198. http://dx.doi.org/10.1074/jbc.271.4.2193

Gerber, S.H., J.C. Rah, S.W. Min, X. Liu, H. de Wit, I. Dulubova, A.C. Meyer, J. Rizo, M. Arancillo, R.E. Hammer, et al. 2008. Conformational switch of syntaxin-1 controls synaptic vesicle fusion. *Science*. 321:1507–1510. http://dx.doi.org/10.1126/science.1163174

Groffen, A.J., S. Martens, R. Díez Arazola, L.N. Cornelisse, N. Lozovaya, A.P. de Jong, N.A. Goriounova, R.L. Habets, Y. Takai, J.G. Borst, et al. 2010. Doc2b is a high-affinity Ca^{2+} sensor for spontaneous neurotransmitter release. *Science*. 327:1614–1618. http://dx.doi.org/10.1126/science.1183765

Hiesinger, P.R., A. Fayyazuddin, S.Q. Mehta, T. Rosenmund, K.L. Schulze, R.G. Zhai, P. Verstreken, Y. Cao, Y. Zhou, J. Kunz, and H.J. Bellen. 2005. The v-ATPase V0 subunit a1 is required for a late step in synaptic vesicle exocytosis in *Drosophila*. *Cell*. 121:607–620. http://dx.doi.org/10.1016/j.cell.2005.03.012

Jahn, R., and D. Fasshauer. 2012. Molecular machines governing exocytosis of synaptic vesicles. *Nature*. 490:201–207. http://dx.doi.org/10.1038/nature11320

Johnson, C.P., and E.R. Chapman. 2010. Otoferlin is a calcium sensor that directly regulates SNARE-mediated membrane fusion. *J. Cell Biol.* 191:187–197. http://dx.doi.org/10.1083/jcb.201002089

Liégeois, S., A. Benedetto, G. Michaux, G. Belliard, and M. Labouesse. 2007. Genes required for osmoregulation and apical secretion in *Caenorhabditis elegans*. *Genetics*. 175:709–724. http://dx.doi.org/10.1534/genetics.106.066035

Lipstein, N., T. Sakaba, B.H. Cooper, K.H. Lin, N. Strenzke, U. Ashery, J.S. Rhee, H. Taschenberger, E. Neher, and N. Brose. 2013. Dynamic control of synaptic vesicle replenishment and short-term plasticity by Ca(2+)-calmodulin-Munc13-1 signaling. *Neuron*. 79:82–96. http://dx.doi.org/10.1016/j.neuron.2013.05.011

Melom, J.E., Y. Akbergenova, J.P. Gavornik, and J.T. Littleton. 2013. Spontaneous and evoked release are independently regulated at individual active zones. *J. Neurosci.* 33:17253–17263. http://dx.doi.org/10.1523/JNEUROSCI.3334-13.2013

Morel, N., J.C. Dedieu, and J.M. Philippe. 2003. Specific sorting of the a1 isoform of the V-H+ATPase a subunit to nerve terminals where it associates with both synaptic vesicles and the presynaptic plasma membrane. *J. Cell Sci.* 116:4751–4762. http://dx.doi.org/10.1242/jcs.00791

Ng, M., R.D. Roorda, S.Q. Lima, B.V. Zemelman, P. Morcillo, and G. Miesenböck. 2002. Transmission of olfactory information between three

populations of neurons in the antennal lobe of the fly. *Neuron*. 36:463–474. http://dx.doi.org/10.1016/S0896-6273(02)00975-3

Nishi, T., and M. Forgac. 2002. The vacuolar (H+)-ATPases—nature's most versatile proton pumps. *Nat. Rev. Mol. Cell Biol.* 3:94–103. http://dx.doi.org/10.1038/nrm729

Pang, Z.P., P. Cao, W. Xu, and T.C. Südhof. 2010. Calmodulin controls synaptic strength via presynaptic activation of calmodulin kinase II. *J. Neurosci.* 30:4132–4142. http://dx.doi.org/10.1523/JNEUROSCI.3129-09.2010

Pang, Z.P., T. Bacaj, X. Yang, P. Zhou, W. Xu, and T.C. Südhof. 2011. Doc2 supports spontaneous synaptic transmission by a Ca^{2+}-independent mechanism. *Neuron*. 70:244–251. http://dx.doi.org/10.1016/j.neuron.2011.03.011

Peri, F., and C. Nüsslein-Volhard. 2008. Live imaging of neuronal degradation by microglia reveals a role for v0-ATPase a1 in phagosomal fusion in vivo. *Cell*. 133:916–927. http://dx.doi.org/10.1016/j.cell.2008.04.037

Perin, M.S., V.A. Fried, D.K. Stone, X.S. Xie, and T.C. Südhof. 1991. Structure of the 116-kDa polypeptide of the clathrin-coated vesicle/synaptic vesicle proton pump. *J. Biol. Chem.* 266:3877–3881.

Peters, C., M.J. Bayer, S. Bühler, J.S. Andersen, M. Mann, and A. Mayer. 2001. Trans-complex formation by proteolipid channels in the terminal phase of membrane fusion. *Nature*. 409:581–588. http://dx.doi.org/10.1038/35054500

Poëa-Guyon, S., M.R. Ammar, M. Erard, M. Amar, A.W. Moreau, P. Fossier, V. Gleize, N. Vitale, and N. Morel. 2013. The V-ATPase membrane domain is a sensor of granular pH that controls the exocytotic machinery. *J. Cell Biol.* 203:283–298. http://dx.doi.org/10.1083/jcb.201303104

Ramirez, D.M., and E.T. Kavalali. 2011. Differential regulation of spontaneous and evoked neurotransmitter release at central synapses. *Curr. Opin. Neurobiol.* 21:275–282. http://dx.doi.org/10.1016/j.conb.2011.01.007

Richmond, J.E., R.M. Weimer, and E.M. Jorgensen. 2001. An open form of syntaxin bypasses the requirement for UNC-13 in vesicle priming. *Nature*. 412:338–341. http://dx.doi.org/10.1038/35085583

Rickman, C., F.A. Meunier, T. Binz, and B. Davletov. 2004. High affinity interaction of syntaxin and SNAP-25 on the plasma membrane is abolished by botulinum toxin E. *J. Biol. Chem.* 279:644–651. http://dx.doi.org/10.1074/jbc.M310879200

Rizo, J., and C. Rosenmund. 2008. Synaptic vesicle fusion. *Nat. Struct. Mol. Biol.* 15:665–674. http://dx.doi.org/10.1038/nsmb.1450

Sara, Y., T. Virmani, F. Deák, X. Liu, and E.T. Kavalali. 2005. An isolated pool of vesicles recycles at rest and drives spontaneous neurotransmission. *Neuron*. 45:563–573. http://dx.doi.org/10.1016/j.neuron.2004.12.056

Saw, N.M., S.Y. Kang, L. Parsaud, G.A. Han, T. Jiang, K. Grzegorczyk, M. Surkont, G.H. Sun-Wada, Y. Wada, L. Li, and S. Sugita. 2011. Vacuolar H(+)-ATPase subunits Voa1 and Voa2 cooperatively regulate secretory vesicle acidification, transmitter uptake, and storage. *Mol. Biol. Cell*. 22:3394–3409. http://dx.doi.org/10.1091/mbc.E11-02-0155

Schneggenburger, R., and E. Neher. 2005. Presynaptic calcium and control of vesicle fusion. *Curr. Opin. Neurobiol.* 15:266–274. http://dx.doi.org/10.1016/j.conb.2005.05.006

Steinhardt, R.A., and J.M. Alderton. 1982. Calmodulin confers calcium sensitivity on secretory exocytosis. *Nature*. 295:154–155. http://dx.doi.org/10.1038/295154a0

Stewart, B.A., H.L. Atwood, J.J. Renger, J. Wang, and C.F. Wu. 1994. Improved stability of *Drosophila* larval neuromuscular preparations in haemolymph-like physiological solutions. *J. Comp. Physiol. A Neuroethol. Sens. Neural Behav. Physiol.* 175:179–191. http://dx.doi.org/10.1007/BF00215114

Strasser, B., J. Iwaszkiewicz, O. Michielin, and A. Mayer. 2011. The V-ATPase proteolipid cylinder promotes the lipid-mixing stage of SNARE-dependent fusion of yeast vacuoles. *EMBO J.* 30:4126–4141. http://dx.doi.org/10.1038/emboj.2011.335

Südhof, T.C., and J.E. Rothman. 2009. Membrane fusion: grappling with SNARE and SM proteins. *Science*. 323:474–477. http://dx.doi.org/10.1126/science.1161748

Sun, J., Z.P. Pang, D. Qin, A.T. Fahim, R. Adachi, and T.C. Südhof. 2007. A dual-Ca^{2+}-sensor model for neurotransmitter release in a central synapse. *Nature*. 450:676–682. http://dx.doi.org/10.1038/nature06308

Wang, D., and P.R. Hiesinger. 2013. The vesicular ATPase: a missing link between acidification and exocytosis. *J. Cell Biol.* 203:171–173. http://dx.doi.org/10.1083/jcb.201309130

Williamson, W.R., and P.R. Hiesinger. 2010. Preparation of developing and adult *Drosophila* brains and retinae for live imaging. *J. Vis. Exp.* 37:e1936.

Williamson, W.R., D. Wang, A.S. Haberman, and P.R. Hiesinger. 2010. A dual function of V0-ATPase a1 provides an endolysosomal degradation mechanism in *Drosophila melanogaster* photoreceptors. *J. Cell Biol.* 189:885–899. http://dx.doi.org/10.1083/jcb.201003062

Wu, M.N., T. Fergestad, T.E. Lloyd, Y. He, K. Broadie, and H.J. Bellen. 1999. Syntaxin 1A interacts with multiple exocytic proteins to regulate neurotransmitter release in vivo. *Neuron*. 23:593–605. http://dx.doi.org/10.1016/S0896-6273(00)80811-9

Xu, J., T. Mashimo, and T.C. Südhof. 2007. Synaptotagmin-1, -2, and -9: Ca(2+) sensors for fast release that specify distinct presynaptic properties in subsets of neurons. *Neuron*. 54:567–581. http://dx.doi.org/10.1016/j.neuron.2007.05.004

Xu, J., Z.P. Pang, O.H. Shin, and T.C. Südhof. 2009. Synaptotagmin-1 functions as a Ca^{2+} sensor for spontaneous release. *Nat. Neurosci.* 12:759–766. http://dx.doi.org/10.1038/nn.2320

Yao, J., J.D. Gaffaney, S.E. Kwon, and E.R. Chapman. 2011. Doc2 is a Ca^{2+} sensor required for asynchronous neurotransmitter release. *Cell*. 147:666–677. http://dx.doi.org/10.1016/j.cell.2011.09.046

Yoshihara, M., Z. Guan, and J.T. Littleton. 2010. Differential regulation of synchronous versus asynchronous neurotransmitter release by the C2 domains of synaptotagmin 1. *Proc. Natl. Acad. Sci. USA*. 107:14869–14874. http://dx.doi.org/10.1073/pnas.1000606107

Zhang, W., D. Wang, E. Volk, H.J. Bellen, P.R. Hiesinger, and F.A. Quiocho. 2008. V-ATPase V0 sector subunit a1 in neurons is a target of calmodulin. *J. Biol. Chem.* 283:294–300. http://dx.doi.org/10.1074/jbc.M708058200

Zhou, P., Z.P. Pang, X. Yang, Y. Zhang, C. Rosenmund, T. Bacaj, and T.C. Südhof. 2013. Syntaxin-1 N-peptide and Habc-domain perform distinct essential functions in synaptic vesicle fusion. *EMBO J.* 32:159–171. http://dx.doi.org/10.1038/emboj.2012.307